Equivalent Transmission Line Models for the Analysis of Edge Effects in Finite Connected and Tightly-Coupled Arrays

Cavallo, Daniele; Syed, Waqas H.; Neto, Andrea

DOI
10.1109/TAP.2017.2670616

Publication date
2016

Document Version
Accepted author manuscript

Published in
IEEE Transactions on Antennas and Propagation

Equivalent Transmission Line Models for the Analysis of Edge Effects in Finite Connected and Tightly-Coupled Arrays

D. Cavallo, *Member, IEEE*, W. H. Syed, *Student Member, IEEE*, and A. Neto, *Fellow, IEEE*

***Abstract*— In this paper we present an analysis of the edge effects in wideband connected arrays of slots and dipoles. Due to the strong mutual coupling between the elements, these arrays can support the propagation of guided waves along their surface. Such waves arise from the edges of the finite array and can be especially detrimental for the performance, since they can travel within the array without geometrical spreading. In this work we introduce Green's function based equivalent transmission line models to describe the propagation of the guided waves. The elements' active impedances are represented as periodic loads on these transmission lines. The equivalent models can be used as a simple and convenient tool to control and minimize the edge effects. Finite array simulations of relevant array structures are discussed. The evidence is that the active impedance and the inter-element capacitance can be tuned to attenuate and reflect the edge-born waves.**

***Index Terms*— Connected arrays, edge effects, finite arrays, truncation effects.**

I. Introduction

CONNECTED arrays have become increasingly popular in the last decade for wideband, wide-scanning phased-array applications. Several designs have been presented in the literature, based on either slot or dipole elements, and have been shown to achieve broad impedance bandwidths within a large scanning range and low cross polarization. Slot-based designs were presented in [1] and more recently in [2], whereas dipole-based arrays were developed in [3]–[6]. By connected-dipole arrays we refer to elements that are either electrically connected or capacitively coupled as originally proposed in [7]: in both configurations, the broadband behavior is achieved by intentionally introducing high mutual coupling between the feeds.

The edge effects in this type of arrays can be especially severe, due to the presence of waves that are generated at the truncated edges of the array and can propagate along the array surface. Although this phenomenon also occurs in narrow-band arrays [8], it is more significant in wideband connected arrays: because of the electrical connection between neighboring feeds, the edge-born waves can propagate almost unattenuated throughout the array aperture and can give rise to strong resonances [9].

Manuscript received Month DD, YYYY; revised Month DD YYYY. First published Month DD, YYYY; current version published Month DD, YYYY. This work was supported by the ERC starting grants ERC-2011-StG Grant AAATSI 278794.

The authors are with the Microelectronics Department of the EEMCS Faculty, Delft University of Technology, 2628 CD Delft, The Netherlands (e-mail: d.cavallo@tudelft.nl).

Color versions of one or more of the figures in this paper are available online at http://ieeexplore.ieee.org.

Digital Object Identifier XX.XXXX/TAP.XXXX.XXXXXXXX.

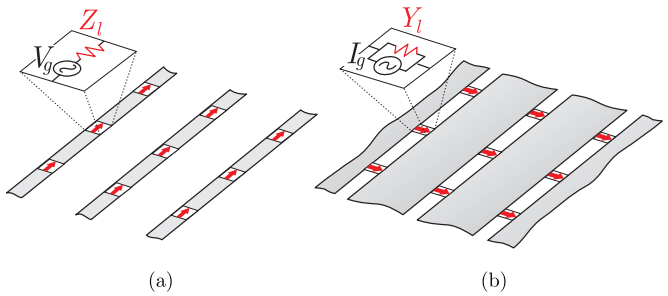

Fig. 1. Connected arrays of (a) dipoles and (b) slots with equivalent generator source and impedance.

In this work, we derive Green's function based equivalent transmission line models to describe the propagation of guided waves along the array surface. These models are useful to clarify the dependence of the propagation from the load impedance of the array elements (Z_l and Y_l in Fig. 1). Such dependence is different for slots and dipoles with consequent implications on the finite array performance.

The influence of the truncation on the active input impedance of the array elements is then investigated in detail. The analysis is based on a numerical spectral domain method derived by the authors in [2], [9] that accounts for the array finiteness. This approach allows, on the one hand, the assessment of the performance of the finite array already at the early design phase and, on the other hand, the simulation of large arrays with minor computational resources.

In Sec. II, the theoretical approach used to derive the equivalent transmission lines is described, considering the canonical cases of a single infinitely long strip in free space and the complementary problem of a single slot. In Sec. III, the same formulation is generalized to different array configurations, and validated by comparison with full-wave simulations performed with a commercial electromagnetic solver. Numerical examples referring to several realistic array structures are reported in Sec. IV, with the aim to provide useful guidelines for the design of connected arrays. Finally conclusions are drawn in Sec. V.

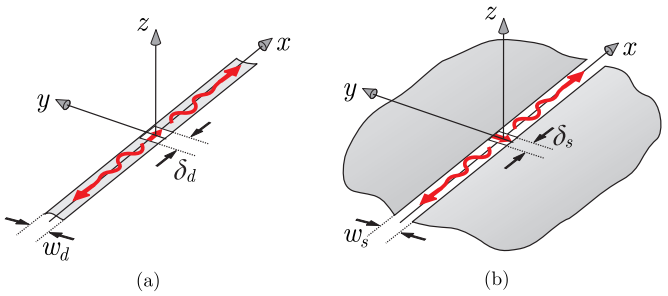

Fig. 2. Single infinitely long (a) dipole and (b) slot in free space.

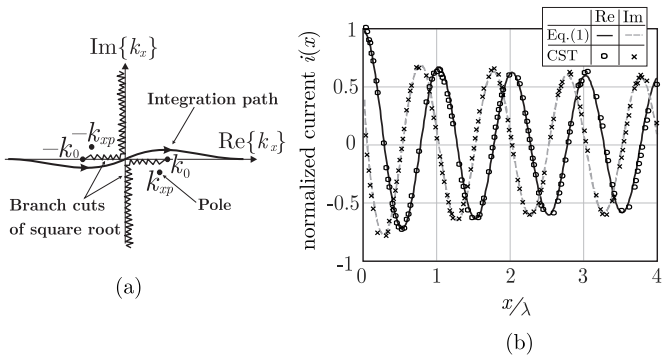

Fig. 3. (a) Singularities on the k_x-complex plane and integration path used to implement (1); (b) normalized current along a strip depicted in Fig. 2(a), for $w_d = \delta_d = \lambda/30$ and $R_d = 0\Omega$: comparison between CST and the numerical integral in (1).

II. Analysis of Single Elements

A peculiar property of connected arrays is the propensity to support guided waves along the array. These waves are generated within the array whenever a discontinuity is present. For instance, if a finite number of feeding ports is considered along the direction of connection, the disrupted periodicity at the edges excites waves that propagate along the array.

To highlight the fundamental edge-effect phenomena occurring in connected arrays, it is helpful to first analyze the case of a single isolated dipole or slot in free space, shown in Fig. 2(a) and (b), respectively.

A. Current on an Infinite Dipole in Free Space

Figure 2(a) shows a single dipole in free space, with infinite length and electrically narrow width w_d, fed with a delta gap of longitudinal dimension δ_d. By applying the separation of variables to the spatial current distribution, the equivalent surface electric current on the strip can be expressed as $j(x,y) = i(x)j_t(y)$, where $j_t(y)$ represents the edge-singular transverse distribution. The x-dependent electric current $i(x)$ can be expressed as an inverse Fourier transform [9], [10]:

$$i(x) = -\frac{1}{2\pi}\int_{-\infty}^{\infty} \frac{V_0 \mathrm{sinc}(\frac{\delta_d}{2}k_x)}{D_d(k_x) - \frac{R_d}{w_d}} e^{-jk_x x} dk_x \qquad (1)$$

where k_x is the spectral counterpart of the spatial variable x and R_d represents a surface resistance, associated with the Ohmic losses of the metal. V_0 is the input voltage across the gap, due to the equivalent Thevenin generator representing the delta-gap excitation (see inset of Fig. 1(a)).

The spectral function $D_d(k_x)$ appearing in the denominator of the integrand in (1) is given by [10], [11]:

$$D_d(k_x) = \frac{1}{2\pi}\int_{-\infty}^{\infty} G_{xx}^{EJ}(k_x,k_y) J_0(\tfrac{w_d}{2}k_y) dk_y = -\frac{\zeta(k_0^2 - k_x^2)}{4k_0} J_0(\tfrac{w_d}{4}\sqrt{k_0^2-k_x^2}) H_0^{(2)}(\tfrac{w_d}{4}\sqrt{k_0^2-k_x^2}). \qquad (2)$$

G_{xx}^{EJ} indicates the xx-component of the spectral dyadic Green's function that relates the electric field to electric sources. J_0 is the zeroth order Bessel function, $H_0^{(2)}$ is the Hankel function of zeroth order and second kind, and ζ and k_0 are the free-space impedance and wavenumber, respectively.

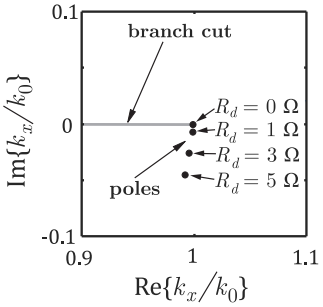

Fig. 4. Positions of the poles of the function $(D_d(k_x) - R_d/w_d)^{-1}$ in the complex plane for different values of the Omhic losses (R_d).

To validate the expression in (1), the integral can be solved numerically by integration over the path depicted in Fig. 3(a). The result of the integration is compared with a simulation performed with CST Microwave Studio [12] in Fig. 3(b), showing good agreement. The curves refer to $R_d = 0\Omega$ and to the geometrical parameters $w_d = \delta_d = \lambda/30$, with λ being the wavelength at the calculation frequency.

It can be noted that the integrand in (1) exhibits branch and polar singularities, associated with the space-wave and modal contributions, respectively. For lossless strips, i.e. $R_d = 0$, it is evident from (2) that the poles coincide with the branch points in $k_x = \pm k_0$. In this case, the residue contribution associated with the polar singularities cannot be extracted and the integral in (1) can only be performed asymptotically (for large values of $|x|$) as described in [13]. However, under the assumption of small but non-zero losses, the poles move slightly away from the branch points of the square root and the residue associated with these poles can be evaluated. To clarify this aspect, Fig. 4 shows the singularities of the function $(D_d(k_x) - R_d/w_d)^{-1}$ in the complex k_x-plane near to the branch point, for different values of R_d, ranging from 0 to 5Ω. The geometrical parameters are set as $w_d = \delta_d = \lambda/30$. It is clear from Fig. 4 that, due to Ohmic losses, the pole k_{xp} moves away from the branch point, and the distance increases proportionally to the surface resistance of the metal strip. Thus, we can calculate the contribution of the integral due to the pole

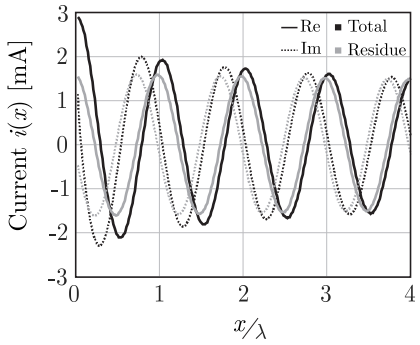

Fig. 5. Comparison between the total current in (1) and the residue contribution in (3), for $w_d = \delta_d = \lambda/30$, $V_g = 1$V and $R_d = 0.25\Omega$.

by applying the residue theorem, leading to

$$i_{\text{res}}(x) = j\frac{V_0 \text{sinc}(\frac{\delta_d}{2}k_{xp})}{D'_d(k_{xp})}e^{-jk_{xp}x} \tag{3}$$

where the prime ($'$) indicates the operation of differentiation. The poles k_{xp} can be easily evaluated by using any local-search algorithm (e.g. Newton's method) to find the zeros of the denominator of the integrand in (1), starting from an initial point near to k_0.

The expression in (3) represents a contribution of the current propagating along the strip that can be associated with a damped wave with very small exponential attenuation due to Ohmic losses. In Fig. 5 the residue contribution is compared to the total current for the same geometry considered in Fig. 3 and setting $R_d = 0.25\Omega$. As expected, the contribution due to the polar singularity represents only a portion of the total current, which also contains the branch-point contribution. However, considering only the residue component is convenient to interpret the propagation along the strip as an equivalent transmission line, as depicted in Fig. 6(a). The physical dimensions of the feed are represented in terms of transformers with turn ratio $n = \text{sinc}(k_{xp}\delta_d/2)$. The characteristic impedance $Z_{0,d}$ of the equivalent transmission line needs to be defined and interpreted.

B. Characteristic Impedance of a Single Infinite Dipole in Free Space

The characteristic impedance is the ratio between voltage and current traveling along the strip $Z_{0,d}(x) = v_{\text{res}}(x)/i_{\text{res}}(x)$. While the expression of $i_{\text{res}}(x)$ was given in (3), we define the residue contribution of the voltage $v_{\text{res}}(x)$ as the integral, from zero to infinity, of the electric field transverse to the direction of propagation. The steps of such calculation are described in Appendix A and lead to

$$Z_{0,d} = \frac{D'_d(k_{xp})}{2j}\,. \tag{4}$$

Equation (4) is consistent with the typical definition of characteristic impedance used for spectral-domain representation of transverse electromagnetic (TEM) or quasi-TEM transmission lines [14]. The function D'_d is defined in (21) in Appendix B, and can be approximated as

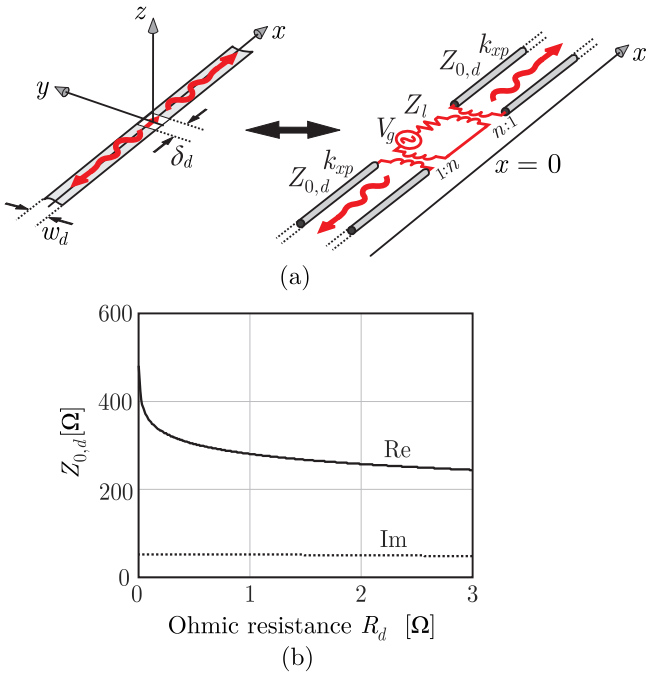

Fig. 6. (a) Equivalent transmission line representing the residue current contribution of a single dipole in free space and (b) characteristic impedance values for $w_d = \lambda/30$ and varying surface resistance R_d.

$$D'_d(k_{xp}) \approx \frac{\zeta k_{xp}}{2k_0}H_0^{(2)}(\tfrac{w_d}{4}\sqrt{k_0^2 - k_{xp}^2}) \tag{5}$$

under the assumption of electrically narrow strip ($w_d \ll \lambda$). It is evident from (5) that only in the case of non-zero losses we can evaluate the derivative, whereas in the absence of losses (for which $k_{xp} = k_0$) we encounter the logarithmic singularity of the Hankel function.

The results for the impedance calculated as in (4) are reported in Fig. 6(b) as a function of the dissipation losses (R_d) for a strip with width $w_d = \lambda/30$. It can be observed that the characteristic impedance exhibits an almost constant imaginary part that can be associated with the lossy (radiative) nature of the propagation along a single strip. This can be easily demonstrated by expanding the Hankel function in (5) for small arguments which leads, after a few algebraic steps reported in Appendix B, to the following expression:

$$Z_{0,d} \approx -\frac{\zeta}{2\pi}\left(\ln\left|\frac{\sqrt{2k_0|\epsilon|}w_d}{8}\right| + \gamma\right) + j\frac{\zeta}{8} \tag{6}$$

where $\epsilon = k_{xp} - k_0$ and $\gamma \approx 0.577$ is the Euler's constant. The constant imaginary part $\text{Im}\{Z_{0,d}\} \approx \zeta/8$ is consistent with the value observed in Fig. 6(b).

C. Single Slot in Free Space

Proceeding in the same manner, we can evaluate the equivalent transmission line of a slot in free space. The steps are very similar to the ones followed for the dipole in the last section and therefore will be omitted. With reference to Fig. 7(a), the transformers have turn ratio $n = \text{sinc}(k_{xp}\delta_s/2)$ and the

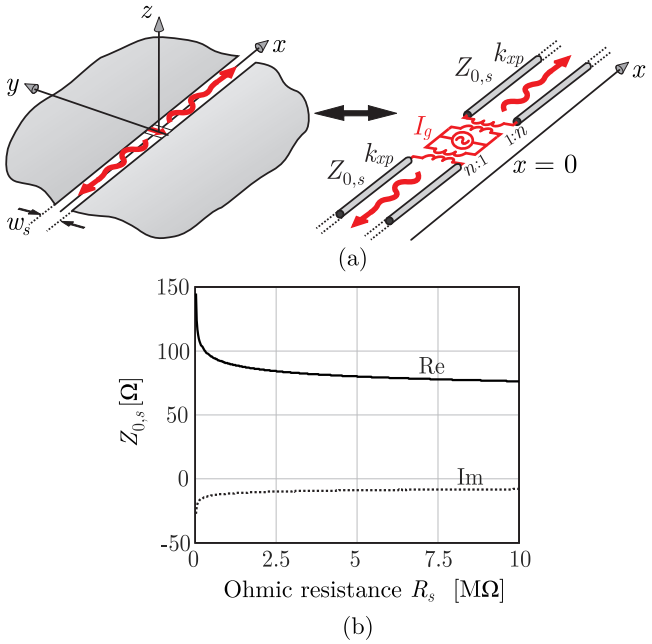

Fig. 7. (a) Equivalent transmission line of a single slot in free space and (b) characteristic impedance for $w_s = \lambda/30$ and varying shunt resistance R_s.

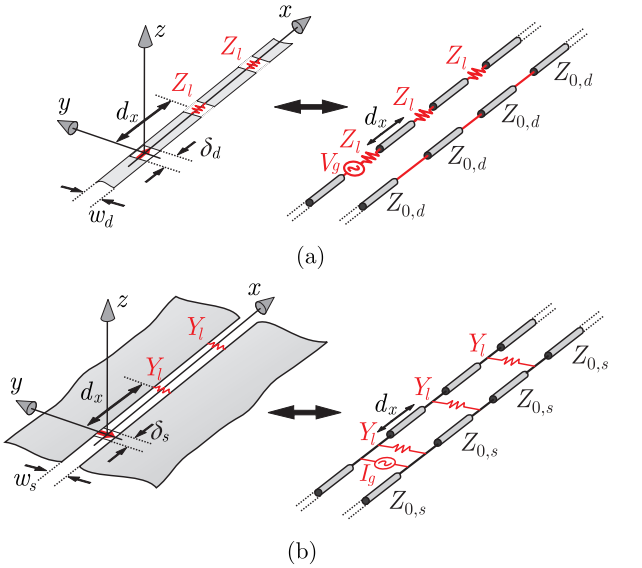

Fig. 8. Geometry and equivalent transmission line of (a) single dipole and (b) single slot with periodic loads.

characteristic impedance of the equivalent transmission line is given by

$$Z_{0,s} = -\frac{2j}{D_s'(k_{xp})} \tag{7}$$

where the function $D_s(k_x)$ is defined as

$$D_s(k_x) = \frac{(k_0^2 - k_x^2)}{\zeta k_0} J_0\left(\tfrac{w_d}{4}\sqrt{k_0^2 - k_x^2}\right) H_0^{(2)}\left(\tfrac{w_d}{4}\sqrt{k_0^2 - k_x^2}\right). \tag{8}$$

The result of the characteristic impedance for a slot of width $w_s = \lambda/30$ is shown in Fig. 7(b), as a function of the losses. For the case of slots, the Ohmic losses of the metal can be represented as an equivalent shunt resistance R_s distributed along the slot length.

III. Analysis of Array Structures

In this section we generalize the equivalent transmission line representation for structures that are closer to realistic array configurations.

A. Dipole and Slot with Periodic Loads

We first consider the case of a single dipole (or slot) with a number of periodically displaced feeds, as shown in Fig. 8. Each feed in a dipole structure consists of a voltage source and a series resistance Z_l, whereas the sources in the slot case can be represented as a current generator with a shunt admittance Y_l. From the point of view of the guided edge-born waves, the periodic feeds represent resistive loads (series for dipole and shunt for slots) located at periodic positions within the equivalent transmission line. The equivalent models are shown in Fig. 8, where we approximated the turn ratio of the transformers as $n \approx 1$. This approximation is valid for electrically small delta-gap feeds.

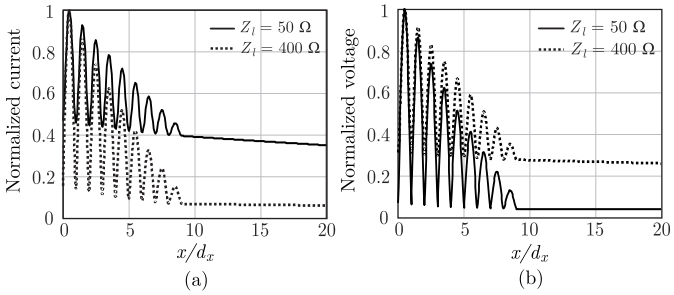

Fig. 9. (a) Normalized current in a dipole loaded periodically with $Z_l = 50\Omega$ and $Z_l = 400\Omega$; (b) normalized voltage in a slot periodic with periodic shunt loads $Z_l = 50\Omega$ and $Z_l = 400\Omega$. Both the dipole and the slot have width $w_d = w_s = \lambda/30$ and are loaded with 9 resistors located at periodic distance $d_x = 0.5\lambda$.

To outline the dependence of the guided waves from the loads, we show in Fig. 9(a) the normalized current magnitude in a dipole loaded with 9 resistors located at periodic distance $d_x = 0.5\lambda$. Two cases are compared, one with $Z_l = 50\Omega$ and $Z_l = 400\Omega$. Stronger attenuation of the current is observed for the higher load resistance, due to power dissipation. On the contrary, the normalized voltage in a slot with periodic shunt loads exhibits an inverse dependence from the load resistance: since the loads are in parallel for the slot case, the voltage correspondent to $Z_l = 50\Omega$ decays faster than the case of $Z_l = 400\Omega$. In both cases (dipoles or slots), the current or the voltage oscillate in the region where the loads are located due to the reflections in each transmission line section that generate standing waves.

B. Two-Dimensional Dipole Array with Backing Reflector

We now consider an array of connected dipoles in the presence of a ground plane (Fig. 10). We assume the array to be infinitely periodic in y, while loaded with a finite number of resistors along x periodically spaced. We assume for simplicity

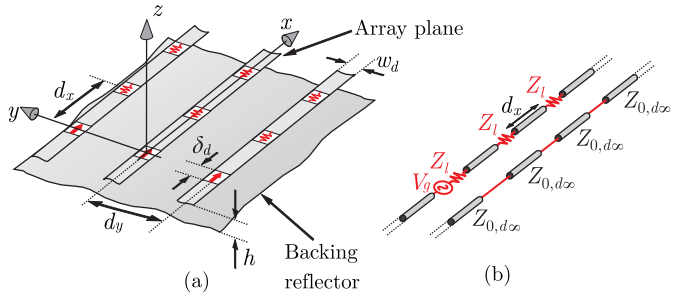

Fig. 10. (a) Connected array of dipoles with ground plane excited at one edge and (b) equivalent transmission line.

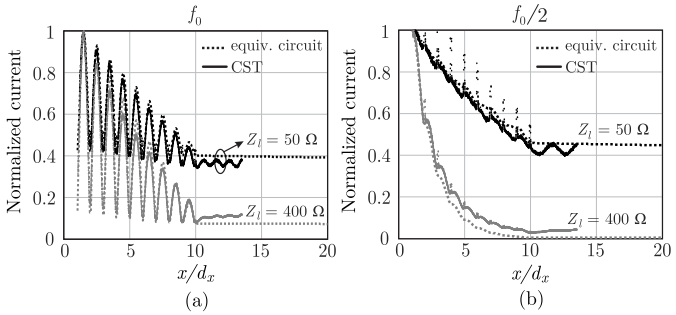

Fig. 11. Normalized current on one of the dipole in the array configuration as in Fig. 10(a). The geometrical parameters are $w_d = \delta_d = \lambda/30$, $h = \lambda/4$, $d_x = d_y = \lambda/2$, with λ being the wavelength at the frequency f_0. Each dipole is loaded with 10 resistors. Current calculated using the transmission line model in Fig. 10(b) is compared with CST simulations, for frequency (a)f_0 and (b)$f_0/2$.

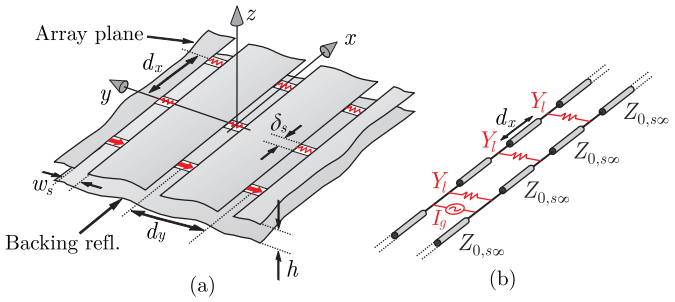

Fig. 12. (a) Connected array of slots with ground plane excited at one edge and (b) equivalent transmission line.

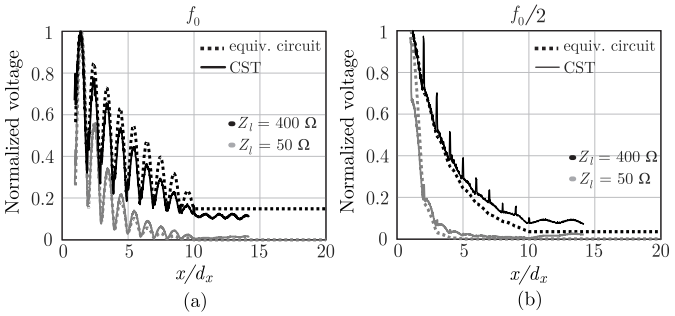

Fig. 13. Normalized voltage on one of the slots in the array configuration as in Fig. 12(a). The geometrical parameters are $w_s = \delta_s = \lambda/30$, $h = \lambda/4$, $d_x = d_y = \lambda/2$, with λ being the wavelength at the frequency f_0. Each slot is loaded with 10 resistors. Voltage calculated using the transmission line model in Fig. 12(b) is compared with CST simulations, for frequency (a)f_0 and (b)$f_0/2$.

that all the dipoles are fed in phase at $x = 0$. The expression of the characteristic impedance of the equivalent transmission line becomes

$$Z_{0,d\infty} = \frac{D'_{d\infty}(k_{xp})}{2j} \tag{9}$$

with

$$D_{d\infty}(k_x) = \frac{1}{d_y} \sum_{m_y=-\infty}^{\infty} G^{EJ}_{\mathrm{BR},xx}(k_x, k_{ym}) J_0(\tfrac{w_d}{2} k_{ym}) \,. \tag{10}$$

$G^{EJ}_{\mathrm{BR},xx}$ indicates the xx-component of the spectral dyadic Green's function for the stratification under analysis, i.e. considering a backing reflector (BR) at distance h from the dipoles. The discrete wavenumber $k_{ym} = -2\pi m_y/d_y$ represents the m_y-th Floquet modes arising from the periodicity along y.

The normalized current on the axis of one of the dipoles in the array configuration is reported in Fig. 11, considering 10 resistors on each dipole. The geometrical parameters are set as $w_d = \delta_d = \lambda/30$, $h = \lambda/4$, $d_x = d_y = \lambda/2$, with λ being the wavelength at the frequency f_0, and the surface resistance of the metal is $R_d = 0.1\Omega$. The current calculated using the transmission line model in Fig. 10(b) is compared with CST simulations, at the frequencies f_0 and $f_0/2$. It can be observed that, as for the single dipole in free-space, the high-resistance loads increase the attenuation rate of the current. There is a good agreement between the full-wave simulations and the simplified transmission line model in the estimation of the current decay.

A number of spikes can be observed in the CST results, in correspondence of the loads. This is because the loads are implemented in CST as a surface resistance distributed on a small square area ($w_d \times w_d$). Since the transverse distributions are different on the metal and the resistive sheets, the value of the current on the dipole axis abruptly peaks in the loads. This effect is not considered in the transmission line model, where the resistors are assumed to be lumped and do not have physical dimensions.

C. Two-Dimensional Slot Array with Backing Reflector

The connected slot array in the presence of a ground plane is depicted in Fig. 12. The expression of the characteristic impedance of the equivalent transmission line is given by

$$Z_{0,s\infty} = -\frac{2j}{D'_{s\infty}(k_{xp})} \tag{11}$$

with

$$D_{s\infty}(k_x) = \frac{1}{d_y} \sum_{m_y=-\infty}^{\infty} G^{HM}_{\mathrm{BR},xx}(k_x, k_{ym}) J_0(\tfrac{w_s}{2} k_{ym}) \tag{12}$$

where $G^{HM}_{\mathrm{BR},xx}$ is the xx-component of the spectral dyadic Green's function linking the magnetic field to the magnetic sources, in the presence of the backing reflector. The normalized voltage on the axis of one of the slots is shown in Fig. 13,

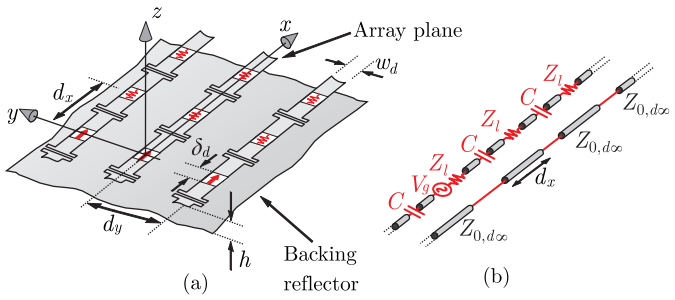

Fig. 14. (a) Array of tightly coupled dipoles with ground plane excited at one edge and (b) equivalent transmission line.

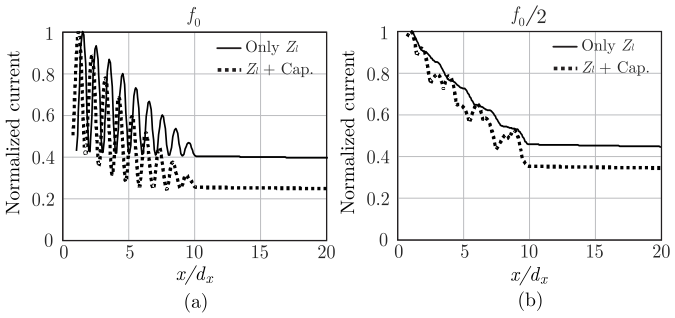

Fig. 15. Normalized current on one of the dipole in the array configuration as in Fig. 14(a). The geometrical parameters are $w_d = \delta_d = \lambda/30$, $h = \lambda/4$, $d_x = d_y = \lambda/2$, with λ being the wavelength at the frequency f_0. Each dipole is loaded with 10 resistors with $Z_l = 50\Omega$. Current calculated using an inter-element capacitance of 0.2 pF are compared with connected dipoles with no capacitance, for frequency (a)$f_0 = 10$ GHz and (b)$f_0/2 = 5$ GHz.

considering 10 resistors on each slot. The parameters are set as $w_s = \delta_d = \lambda/30$, $h = \lambda/4$, $d_x = d_y = \lambda/2$, $R_s = 10^5\Omega$. Unlike the dipole structure, the low-resistance loads increase the attenuation rate of the voltage, being in parallel to the transmission line. There is a good agreement between the full-wave simulations and the simplified transmission line model.

D. Tightly Coupled Array with Backing Reflector

Another relevant case to investigate is the configuration when the array of dipoles includes inter-element capacitance, to realize the so-called tightly-coupled array concept [4]. In Fig. 14(a) the geometry of the capacitively-coupled dipoles in the presence of a ground plane is shown. The equivalent transmission line model becomes the one in Fig. 14(b) where, in addition to the periodic resistive loads, also series capacitances are present along the line. To understand the effect of the capacitance on the waves propagating along the array, we report in Fig. 15 the normalized current on the strip, comparing the case of connected dipoles (Figs. 10 and 11) with the case when the same array includes an inter-element capacitance $C = 0.2$ pF. The frequencies of calculation are $f_0 = 10$ GHz and $f_0/2 = 5$ GHz. It can be noted that the presence of the additional series capacitance results in a comparatively faster decay of the current magnitude, because of the increased reflection in the transmission line sections.

IV. Investigation on the Array Active Impedance

In this section, the finite edge effects in connected arrays are investigated by quantifying the variation of the active voltage standing wave ratio (VSWR) within the arrays. Simulations of finite×infinite arrays are performed using the semi-analytical solutions developed in [2], [9], [15]. The active VSWR for arrays composed by $9 \times \infty$ elements is shown in Fig. 16 and compared with the infinite array solution. To highlight the dependence of the edge effects from the matching impedance of the elements, we consider three cases:

1) Connected array of dipoles in the presence of a backing reflector (inset of Fig. 16(a)), normalized to input impedance $Z_l = 400\Omega$.
2) Array of capacitively-coupled dipoles in the presence of a backing reflector and loaded with a dielectric slab (inset of Fig. 16(b)), normalized to input impedance $Z_l = 100\Omega$.
3) Connected array of slots in the presence of a backing reflector and loaded with a dielectric slab (inset of Fig. 16(c)), normalized to input impedance $Z_l = 100\Omega$.

These three example have been selected because they all exhibit bandwidths of at least one octave. The periods are $d_x = d_y = 8.43$mm for all the geometries and the arrays scan to $\theta = 30°$ in the plane $\varphi = 0$. The distance from the ground plane is 4.7mm in all cases and the dielectric slabs have height of 2.8mm and relative permittivity of $\varepsilon_r = 2.2$. The presence of the dielectric superstrate allows to reduce the active input impedance, that normally is close to the free-space impedance (377Ω), to values of about 100Ω.

It is apparent that case 1 in Fig. 16(a) exhibits the smallest variation of VSWR within the finite array. This is accordant with the interpretation of the edge-effect phenomenon that we gave in the previous sections. The edge-born waves quickly attenuate along the array due to the high-resistance series loads ($Z_l = 400\Omega$). From Fig. 16(b) it can be noted that, although significantly wider bandwidth is obtained because of the presence of the inter-element capacitance, higher variations of VSWR occur and some of the edge-element curves appreciably diverge at lower frequencies from the infinite array case. This is in line with the observation that low impedance values for the port terminations do not attenuate the edge waves effectively. Fluctuations of VSWR are also found for the slot case in Fig. 16(c), with values remaining within a ± 0.6 range around the infinite array solution.

V. Conclusions

We presented an investigation on the edge effects occurring in wideband connected arrays of slots and dipoles. The analysis is based on closed-form solutions derived from the spectral Green's function of connected arrays. The fundamental wave propagation phenomena were described in terms of equivalent transmission lines. The port impedance of each element was shown to represent a series load for dipoles, whereas a shunt load for slots. For this reason dipole arrays matched to low impedances support almost unattenuated propagation of edge-born guided waves along the aperture, which deteriorate the finite array performance. On the contrary, slot designs with

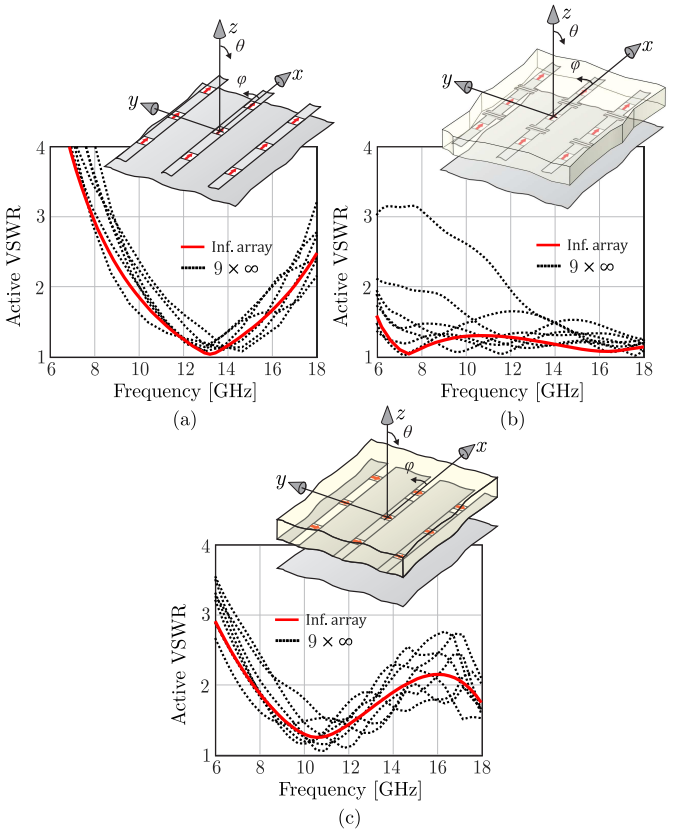

Fig. 16. Active VSWR for the elements of $9 \times \infty$ arrays, scanning to $\theta = 30°$ in the plane $\varphi = 0$, compared with infinite array solution: (a) array of connected dipoles, with 400Ω input impedance; (b) array of capacitively-coupled dipoles with a superstrate, matched to 100Ω; (c) array of connected slots with superstrate, matched to 100Ω.

low impedance strongly reflect the guided waves that remain confined only at the edge elements. Capacitances between adjacent array elements, as in tightly coupled arrays, can also help attenuate the edge waves.

Numerical results of the active VSWR of finite connected arrays were presented to support the theoretical analysis.

Appendix A
Voltage Solution for a Single Dipole as Integral of the Transverse Field

To find a value of the characteristic impedance associated with a single strip in free space, it is convenient to interpret the voltage wave traveling along the strip as the integral of the electric transverse field along a line that goes from the dipole to infinity:

$$v_{\text{res}}(x) = -\int_0^\infty e_y(x,y)dy \tag{13}$$

where e_y represents the y-component of the spatial electric field. By expressing the field as an inverse Fourier transform of its spectrum E_y, one obtains

$$v_{\text{res}}(x) = -\int_0^\infty \frac{1}{4\pi^2}\iint_{-\infty}^{\infty} E_y(k_x,k_y)e^{-jk_x x}e^{-jk_y y}dk_x dk_y dy\,. \tag{14}$$

The spectrum is given by

$$E_y(k_x,k_y) = I(k_x)J_0(\tfrac{w_d}{2}k_y)G_{yx}^{EJ}(k_x,k_y) \tag{15}$$

where G_{yx}^{EJ} is the yx-component of the spectral dyadic Green's function. By substituting $I(k_x)$ from (1) in (14), and writing explicitly the Green's function, the voltage can be expressed, after a few algebraic steps, as

$$v_{\text{res}}(x) = \frac{1}{4\pi^2}\iint_{-\infty}^{\infty} \frac{V_0\text{sinc}(\frac{\delta_d}{2}k_x)}{D_d(k_x) - \frac{R_d}{w_d}} J_0\left(\frac{w_d}{2}k_y\right) \cdot \frac{\zeta}{2k_0}\frac{k_x k_y}{k_z}e^{-jk_x x}\left(\int_0^\infty e^{-jk_y y}dy\right)dk_x dk_y\,. \tag{16}$$

To satisfy the radiation condition, we impose $\lim_{y\to\infty} e^{-jk_y y} = 0$. Thus performing the integration in y, (16) becomes

$$v_{\text{res}}(x) = -j\frac{\zeta}{4k_0}\frac{1}{2\pi}\int_{-\infty}^{\infty} \frac{V_0\text{sinc}(\frac{\delta_d}{2}k_x)}{D_d(k_x) - \frac{R_d}{w_d}} \cdot \left(\frac{1}{\pi}\int_{-\infty}^{\infty}\frac{J_0\left(\frac{w_d}{2}k_y\right)}{k_z}dk_y\right)k_x e^{-jk_x x}dk_x\,. \tag{17}$$

By using the closed form solution of the integral between parenthesis [16] and applying the residue theorem, we obtain

$$v_{\text{res}}(x) = -V_0\text{sinc}(\tfrac{\delta_d}{2}k_x) \frac{\frac{\zeta k_{xp}}{4k_0}J_0\left(\frac{w_d}{4}\sqrt{k_0^2-k_{xp}^2}\right)H_0^{(2)}\left(\frac{w_d}{4}\sqrt{k_0^2-k_{xp}^2}\right)}{D_d'(k_{xp})}e^{-jk_{xp}x}\,. \tag{18}$$

Finally, by substituting (5) in (18), the voltage can be expressed as

$$v_{\text{res}}(x) = -\frac{1}{2}V_0\text{sinc}(\tfrac{\delta_d}{2}k_{xp})e^{-jk_{xp}x}\,. \tag{19}$$

Appendix B
Derivative of $D_d(k_x)$ and Small-Loss Approximation of the Characteristic Impedance

The derivative of the spectral function $D_d(k_x)$ in (2) is given by

$$D_d'(k_x) = -\frac{\zeta}{4k_0}\cdot \frac{d}{dk_x}\left[(k_0^2-k_x^2)J_0\left(\tfrac{w_d}{4}\sqrt{k_0^2-k_x^2}\right)H_0^{(2)}\left(\tfrac{w_d}{4}\sqrt{k_0^2-k_x^2}\right)\right]\,. \tag{20}$$

To simplify the notation, let us define $K = (k_0^2-k_x^2)^{1/2}$. For electrically narrow strips, we can approximate $J_0(Kw_d/4) \approx 1$, leading to

$$\begin{aligned} D_d'(k_x) &\approx -\frac{\zeta}{4k_0}\frac{d}{dk_x}\left[K^2H_0^{(2)}\left(\tfrac{w_d}{4}K\right)\right] = \\ &= -\frac{\zeta}{4k_0}\frac{d}{dK}\left[K^2H_0^{(2)}\left(\tfrac{w_d}{4}K\right)\right]\frac{dK}{dk_x} = \\ &= \frac{\zeta k_x}{2k_0}\left[H_0^{(2)}\left(\tfrac{w_d}{4}K\right) - \frac{w_d}{8}KH_1^{(2)}\left(\tfrac{w_d}{4}K\right)\right]\,. \end{aligned} \tag{21}$$

By neglecting the term proportional to K, we can express (21) as

$$D'_d(k_x) \approx \frac{\zeta k_x}{2k_0} H_0^{(2)}\left(\tfrac{w_d}{4}K\right) . \quad (22)$$

The Hankel function can be approximated with its expansion for small arguments:

$$D'_d(k_{xp}) \approx \frac{\zeta}{2}\frac{k_0+\epsilon}{k_0}\left[1-\frac{2j}{\pi}\left(\ln(\tfrac{\sqrt{k_0^2-k_{xp}^2}w_d}{8})+\gamma\right)\right] \quad (23)$$

where we evaluated the derivative in the pole $k_{xp} = k_0 + \epsilon$ with $\epsilon \ll k_0$ in the case of small losses. In (23) we used the Euler's constant $\gamma \approx 0.577$. The square root can be written as

$$k_{zp} = \pm\sqrt{k_0^2-k_{xp}^2} = \pm\sqrt{k_0^2-(k_0+\epsilon)^2} = \pm\sqrt{-2k_0\epsilon-\epsilon^2}$$
$$\approx \pm\sqrt{-2k_0\epsilon} = \pm j\sqrt{2k_0|\epsilon|}e^{j\angle\epsilon/2} . \quad (24)$$

The sign of the square root is chosen so that $\mathrm{Im}(k_z) < 0$, which gives

$$k_{zp} = \sqrt{2k_0|\epsilon|}e^{j(\angle\epsilon/2-\pi/2)} \approx \sqrt{2k_0|\epsilon|}e^{-j3\pi/4} \quad (25)$$

since ϵ is almost a purely imaginary number lower than 0, thus $\angle\epsilon \approx -\pi/2$. By substituting (25) in (23), and performing some algebraic manipulations, we obtain

$$D'_d(k_{xp}) \approx -j\frac{\zeta}{\pi}\ln\left|\frac{\sqrt{2k_0|\epsilon|}w_d}{8}\right| - j\frac{\zeta}{\pi}\gamma - \zeta/4 \quad (26)$$

which leads to the approximated expression of the characteristic impedance

$$Z_{0,d} = \frac{D'_d(k_{xp})}{2j} \approx -\frac{\zeta}{2\pi}\left(\ln\left|\frac{\sqrt{2k_0|\epsilon|}w_d}{8}\right|+\gamma\right)+j\frac{\zeta}{8} . \quad (27)$$

The approximated characteristic admittance for the slot case can be evaluated in a similar manner:

$$Z_{0,s} = \frac{-2j}{D'_s(k_{xp})} \approx \zeta\frac{1}{-\frac{2}{\pi}\left(\ln\left|\frac{\sqrt{2k_0|\epsilon|}w_s}{8}\right|+\gamma\right)+j\frac{1}{2}} . \quad (28)$$

REFERENCES

[1] J. J. Lee, S. Livingston, R. Koenig, D. Nagata, and L. L. Lai, "Compact light weight UHF arrays using long slot apertures," *IEEE Trans. Antennas Propag.*, vol. 54, no. 7, pp. 2009-2015, Jul. 2006.

[2] W. H. Syed, D. Cavallo, H. Thippur Shivamurthy, and A. Neto, "Wideband, wide-scan planar array of connected slots loaded with artificial dielectric superstrates," *IEEE Trans. Antennas Propag.*, vol. 64, no. 2, pp. 543-553, Feb. 2016.

[3] S. S. Holland, D. H. Schaubert, and M. N. Vouvakis, "A 7-21 GHz dual-polarized planar ultrawideband modular antenna (PUMA) array," *IEEE Trans. Antennas Propag.*, vol. 60, no. 10, pp. 4589-4600, Oct. 2012.

[4] J. P. Doane, K. Sertel, and J. L. Volakis, "A wideband, wide scanning tightly coupled dipole array with integrated balun (TCDA-IB)," *IEEE Trans. Antennas Propag.*, vol. 61, no. 9, pp. 4538-4548, Sep. 2013.

[5] D. Cavallo, A. Neto, G. Gerini, A. Micco, and V. Galdi, "A 3 to 5 GHz wideband array of connected dipoles with low cross polarization and wide-scan capability," *IEEE Trans. Antennas Propag.*, vol. 61, no. 3, pp. 1148-1154, Mar. 2013.

[6] R. J. Bolt, D. Cavallo, G. Gerini, D. Deurloo, R. Grooters, A. Neto, and G.Toso, "Characterization of a dual-polarized connected-dipole array for Ku-band mobile terminals," *IEEE Trans. Antennas Propag.*, vol. 64, no. 2, pp. 391-398, Feb. 2016.

[7] B. A. Munk, *Finite Antenna Array and FSS.*, John Wiley & Sons, Inc., Hoboken, NJ, USA, 2003.

[8] O. A. Civi and P. H. Pathak, "Array guided surface waves on a finite planar array of dipoles with or without a grounded substrate," *IEEE Trans. Antennas Propag.*, vol. 54, no. 8, pp. 2244-2252, Aug. 2006.

[9] A. Neto, D. Cavallo, and G. Gerini, "Edge-born waves in connected arrays: A finite infinite analytical representation," *IEEE Trans. Antennas Propag.*, vol. 59, no. 10, pp. 3646-3657, Oct. 2011.

[10] A. Neto, D. Cavallo, G. Gerini, and G. Toso, "Scanning performances of wideband connected arrays in the presence of a backing reflector," *IEEE Trans. Antennas Propag.*, vol. 57, no. 10, pp. 3092-3102, Oct. 2009.

[11] A. Neto and J. J. Lee, "Ultrawide-band properties of long slot arrays," *IEEE Trans. Antennas Propag.*, vol. 54, no. 2, pp. 534-543, Feb. 2006.

[12] *CST Microwave Studio* 2014 [Online]. Available: http://www.cst.com

[13] D. S. Jones, *Methods in Electromagnetic Wave Propagation, 2nd Ed.* IEEE Press, New York, USA, 1994.

[14] N. Das, "A new theory of the characteristic impedance of general printed transmission lines applicable when power leakage exists," *IEEE Trans. Microw. Theory Techn.*, vol. 48, no. 7, pp. 1108-1117, Jul 2000.

[15] D. Cavallo, A. Neto, and G. Gerini, "Analytical description and design of printed dipole arrays for wideband wide-scan applications," *IEEE Trans. Antennas Propag.*, vol. 60, no. 12, pp. 6027-6031, Dec. 2012.

[16] I. S. Gradshteyn and I. M. Ryzhik, *Table of Integrals, Series, and Products, 7th Ed.* Elsevier Inc., Burlington, MA, USA, 2007.

Daniele Cavallo (S'09−M'11) received the M.Sc. degree (*summa cum laude*) in telecommunication engineering from the University of Sannio, Benevento, Italy, in 2007, and his Ph.D. degree (*cum laude*) in electromagnetics from Eindhoven University of Technology (TU/e), Eindhoven, The Netherlands, in 2011.

From 2007 to 2011, he was with the Antenna Group at the Netherlands Organization for Applied Scientific Research (TNO), The Hague, The Netherlands. In the years 2012-2015, he was Post-Doctoral researcher in the Microelectronics department of Delft University of Technology (TUDelft), Delft, The Netherlands. During 2015, he spent two months as a visiting researcher at Chalmers University of Technology in Gothenburg, Sweden. From September 2015, he is assistant professor in the Terahertz Sensing Group at TUDelft. He is the author or coauthor of about 90 papers published in peer-reviewed international journals and conference proceedings. His research interests include analytical and numerical methods for antenna characterization, the design of antenna arrays and high-frequency on-chip antennas.

Dr. Cavallo was first author of the paper awarded with the best innovative paper prize at the 30th ESA Antenna Workshop in 2008 and nominee for the best doctoral project in the TU/e Academic Annual Awards 2012. He has been awarded a three-year personal grant from the Netherlands Organization for Scientific Research (NWO VENI, 250 keuro), for developing "Efficient On-Chip Antennas for Terahertz Applications". He is currently an Associate Editor of the IEEE TRANSACTIONS ON ANTENNAS AND PROPAGATION. He is a member of the European Association on Antennas and Propagation (EurAAP).

Waqas H. Syed (S'11) received the B.Sc. degree with distinction in telecommunication engineering from the CIIT, Islamabad, Pakistan, in 2007, his M.Sc. degree from RWTH Aachen University, Aachen, Germany, in 2010, and his Ph.D. degree (*cum laude*) in electromagnetics from Delft University of Technology (TUDelft), Delft, The Netherlands, in 2015.

From 2015 to 2016, he was Post-Doctoral researcher in the Terahertz Sensing Group at TUDelft. He is currently working as an antenna engineer at NXP Semiconductors, Eindhoven, The Netherlands. His research interests include artificial dielectrics and the design of integrated antennas and arrays.

Dr. Syed was recipient of the Special Mention for Excellent Presentation at the European Conference on Antennas and Propagation (EuCAP) in 2015. He was also the recipient of the 2016 Else Kooi Award for the Best Young Researcher in the field of applied semiconductor research and microelectronics conducted in the Netherlands.

Andrea Neto (M'00−SM'10−F'16) received the Laurea degree (*summa cum laude*) in electronic engineering from the University of Florence, Florence, Italy, in 1994 and the Ph.D. degree in electromagnetics from the University of Siena, Siena, Italy, in 2000.

Part of his Ph.D. degree was developed at the European Space Agency Research and Technology Center, Noordwijk, The Netherlands, where he worked for the antenna section for over two years. In the years 2000−2001, he was a Post-Doctoral Researcher at the California Institute of Technology, Pasadena, CA, USA, working for the Sub-Millimeter-Wave Advanced Technology Group. From 2002 to January 2010, he was a Senior Antenna Scientist at TNO Defence, Security, and Safety, The Hague, The Netherlands. In February 2010, he was appointed Full Professor of Applied Electromagnetism in the Electrical Engineering, Mathematics and Computer Science Department, Technical University of Delft, Delft, The Netherlands, where he formed and leads the THz Sensing Group. His research interests are in the analysis and design of antennas, with emphasis on arrays, dielectric lens antennas, wideband antennas, EBG structures, and THz antennas.

Prof. Neto was corecipient of the H. A. Wheeler award for the best applications paper of the year 2008 in the IEEE TRANSACTIONS ON ANTENNAS AND PROPAGATION. He was corecipient of the best innovative paper prize at the 30th ESA Antenna Workshop in 2008. He was corecipient of the best antenna theory paper prize at the European Conference on Antennas and Propagation (EuCAP) in 2010. He served as an Associate Editor of the IEEE TRANSACTIONS ON ANTENNAS AND PROPAGATION (2008−2013) and IEEE ANTENNAS AND WIRELESS PROPAGATION LETTERS (2005-2013). He now serves as an Associate Editor of the IEEE TRANSACTIONS ON TERAHERTZ SCIENCE AND TECHNOLOGY. He is member of the Technical Board of the European School of Antennas and organizer of the course on Antenna Imaging Techniques. He is a member of the steering committee of the network of excellence NEWFOCUS, dedicated to focusing techniques in mm and sub-millimeter-wave regimes. In 2011 he was awarded the European Research Council Starting Grant to perform research on Advanced Antenna Architectures for THz Sensing Systems. He was the Awards and Grants Chair for EUCAP 2014.